Relating Chemical Structure to Device Performance via Morphology Control in Diketopyrrolopyrrole-Based Low Band Gap Polymers

Feng Liu,[†] Cheng Wang,[‡] Jayanta K. Baral,[†] Lei Zhang,[†] James J. Watkins,[†] Alejandro L. Briseno,*[†] and Thomas P. Russell*[†]

[†]Department of Polymer Science and Engineering, University of Massachusetts Amherst, Amherst, Massachusetts 01003, United States

[‡]Advanced Light Source, Lawrence Berkeley National Laboratory, Berkeley, California 94720, United States

ⓢ Supporting Information

ABSTRACT: We investigated the structure–morphology–performance relationship of diketopyrrolopyrrole (DPP)-based low band gap polymers with different donor cores in organic field effect transistors (OFETs) and organic photovoltaics (OPVs). The change in the chemical structure led to strong physical property differences, such as crystalline behavior, blend morphology, and device performance. In addition, the choice of solvents and additives enabled one to fine tune the properties of these materials in the condensed state. For instance, when thin films were processed from solvent mixtures, both in the pure polymer and in a blend, we observed an enhanced edge-on orientation and the formation of thinner and longer polymer fibrils. In the BHJ blends, processing from a solvent mixture reduced the size scale of the phase separation and promoted the formation of a fibrillar network morphology, having a polymer–PCBM mixture filling the interfibrillar regions. The characteristic length scale of the fibrillar network dictated the specific inner surface area, which directly correlated to the performance in the OPV devices. When the BHJ mixture was processed from a single solvent, a large-scale phase separated morphology was observed that was stratified, normal to the film surface. A strong scattering anisotropy was observed in the resonant soft X-ray scattering of the blends that provided insight into the packing of the polymer chains within the fibrils. The morphology and performance trend in OPVs paralleled the performance in an OFET, suggesting that similar processing conditions should be considered in OFET fabrication.
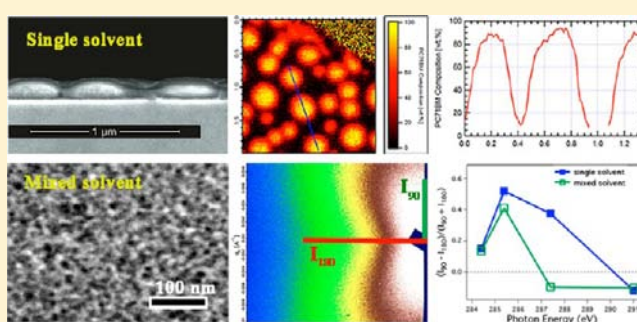
■ INTRODUCTION

Conjugated polymers have attracted much attention in the past decades due to their promising applications in new technologies, such as light emitting diodes, organic field effect transistors (OFETs), and organic photovoltaics (OPVs). Polymer-based bulk heterojunction (BHJ) solar cells have surpassed a 9% power conversion efficiency for single-layer devices[1] and the field effect mobility has reached 10 cm^2 V^{-1} s^{-1}.[2] In the course of performance optimization, a large number of conjugated polymers have been developed, among which low band gap polymers have proven to be quite promising for both OPVs and OFETs.[3] By tailoring the chemical composition of the polymer or copolymer, the energy levels, absorption spectra, and molecular packing can be fine tuned to suit specific device configurations.[4] In the development of low band gap (LBG) polymers, an electron rich donor unit is coupled with an electron deficient unit to reduce the absorption band gap and enhance the intermolecular interaction.[5,6] Other factors, such as self-assembly properties, solubility, molecular weight, and crystallinity, must also be considered to optimize performance.[7]

For conjugated polymers employed in OFETs, major factors that determine the device performance include chain packing/orientation and crystallinity within the active layer[8–13] and, most importantly, at the active layer/dielectric interface.[14–17] In BHJ solar cell devices, the active layer morphology is more complex. A bicontinuous network composed of a phase-separated donor polymer and acceptor material, with each domain having the characteristic length scales of ~10–20 nm, is needed to effectively split the excitons and transport the carriers to their respective electrodes.[7,18,19] Optimizing device performance further mandates a synergistic interactive development between synthesis and morphological characterization so as to fully understand the coupling between chemical structure and morphology and, thereby, enable informed molecular design.

Conjugated polymers incorporating diketopyrrolopyrrole (DPP) units are an interesting family of LBG polymers,[20–26] which show long wavelength absorption and good mobility.[27–29] A 6.5% PCE has been reported for single-layered OPV devices.[30] However, generating suitable thin film morphologies requires the use of an additive or a solvent mixture.[24–26,31] This

additive approach mediates the scale of the phase-separated morphology and the aggregation of polymer chains in solution. In this study, we compare the molecular structure of three DPP polymers to their physical properties/morphology and device performance as a function of solvent and additive processing conditions. We show that chemical structure modification and processing conditions are equally important for the optimization of the morphology. The miscibility of the components also plays an important role in defining the morphology of thin films prepared from a single solvent. While this contributes to the morphology of thin film mixtures, the ordering (crystallization) of the polymer in the presence of the solvent additive is found to dictate the morphology, establishing a framework that dictates the ultimate morphology and performance.

■ RESULTS AND DISCUSSION

Polymer Absorption. The chemical structure of the three conjugated polymers: poly(diketopyrrolopyrrole-thiophene-fluorene-thiophene) (**DPPF**), poly(diketopyrrolopyrrole-terthiophene) (**DPPT**), and poly(diketopyrrolopyrrole-quaterthiophene) (**DPPBT**) that were used in this study are shown in Figure 1. DPPF and DPPT were soluble in common organic
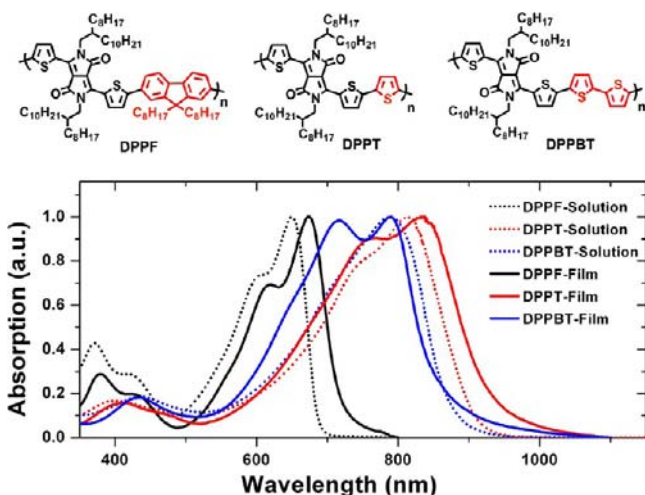

Figure 1. Polymer structure and UV−vis absorption in solution and thin film.

solvents, like chloroform (CF) and chlorobenzene (CB). DPPBT was soluble in chloroform, but its solubility in chlorobenzene and 1,2-dichlorobenzene (DCB) was limited. Figure 1 shows the UV−vis absorption spectra of the three DPP-based polymers in solution and in thin films. Due to the electron deficient nature of the DPP unit, its copolymers with an electron-donating unit show long wavelength absorption. As seen in Figure 1, when copolymerized with fluorene, an absorption band at 650 nm was observed in solution, due to the characteristic electronic neutrality of fluorene and the large rotation angle between the monomers. When the thiophene unit was used, a surprisingly longer wavelength absorption was observed with a maximum at 815 nm, which was 25 nm deeper than that of the DPP−bithiophene copolymer. In going from the solution to the solid or condensed state, a 25 nm red shift was observed for the DPPF-based polymer and a 20 nm red-shift for the DPPT-based, due to a decrease in rotation angle along the backbone and an enhanced packing. For the DPPBT-based polymer, no red-shift was observed. However, a new

absorption appeared at 715 nm, due to the formation of H aggregates.[32] Although DPPT and DPPBT absorption absorbed strongly from 650 to 850 nm, the absorption in the shorter wavelength region was limited. Consequently, $PC_{71}BM$ was used to complement the absorption in this region.

Charge Transport Properties. Charge carrier motilities of DPP polymers were evaluated using bottom contact/top gate (BC/TG) and top contact/bottom gate (TC/BG) OFET devices (Figure 2a). Device fabrication details can be found in Supporting Information.[33] Device measurements were performed at ambient conditions using a standard probe station and a Keithly 4200 SCS semiconductor analyzer. To control the thin film morphology, both single and mixed solvent processing were used (DPPF and DPPT showed good solubility in chlorobenzene, so chlorobenzene was used as the primary solvent, and 1,8-diiioctane (DIO, 3 v%) was used as an additive). DPPBT showed good solubility in chloroform, so chloroform was used as primary solvent and 1,2-dichlorobenzene (20 v%) was used as additive. In bottom contact/top gate (BC/TG) devices, amorphous fluoropolymer CYTOP was used as the dielectric, and in top contact/bottom gate (TC/BG) devices, SiO_2 (300 nm) was used as the dielectric. DPP polymer thin films were spin coated from 5 to 8 mg/mL solutions at 1500 rpm for a minute. Afterward, the films were further dried under vacuum for more than 12 h and then transfer printed onto devices.[34] Hole mobilities were calculated in the saturation regime. The device output and transfer characteristics are given in Table 1 and Figure 2b,c (We only show DPPBT bottom contact/top gate devices as a representation). As can be seen from the tabulated results, the CYTOP dielectric gave much better performance, in comparison to SiO_2. This can be attributed to the low polarity of CYTOP and better contacts between the dielectric and semiconductor layer.[17,35] Thin films processed from a solvent mixture showed much better mobilities, which can be directly correlated with the improved structural order of the thin films. For DPPBT, the mobility obtained from films processed with a solvent mixture yielded mobilities up to 1.2 cm^2 V^{-1} s^{-1}. For the annealing free devices, this mobility is already quit high, and equally important, the use of a processing additive affords a new handle for optimizing the performance of OFETs.

Structure Order of Polymer Thin Films. The structure of the conjugated polymer within the thin film influences the transport properties of the material. The structure was characterized using grazing incidence X-ray diffraction (GIXD).[36] Figure 3 shows the 2D GIXD profiles of the polymer films investigated here. The out-of-plane line cuts are shown in Figure S1. As can be seen, modifying the chemical structure and processing conditions have equally important effects on the solid-state packing of polymer chains. Single-solvent processed DPPF thin films were highly amorphous, exhibiting only a weak peak at ∼0.32 A^{-1}, corresponding to a spacing of 1.96 nm. However, when we switched to CB/DIO processing, a sharp peak at 0.37 A^{-1} (1.7 nm) was seen. This arises from the (100) interchain packing. DPPF has a larger alkyl side chain (C12) in the DPP unit (100) with a spacing of 1.96 nm. A reduced (100) spacing in solvent mixture processing indicates those alkyl chains better interdigitated and crystallized.[37] The in-plane diffraction showed a small peak at 0.5 A^{-1}, arising from the side chain crystallization. A weak π−π stacking is seen for the CB/DIO-processed films with a characteristic distance of 0.39 nm. The enhanced crystallization of DPPF using the solvent mixture processing was the major
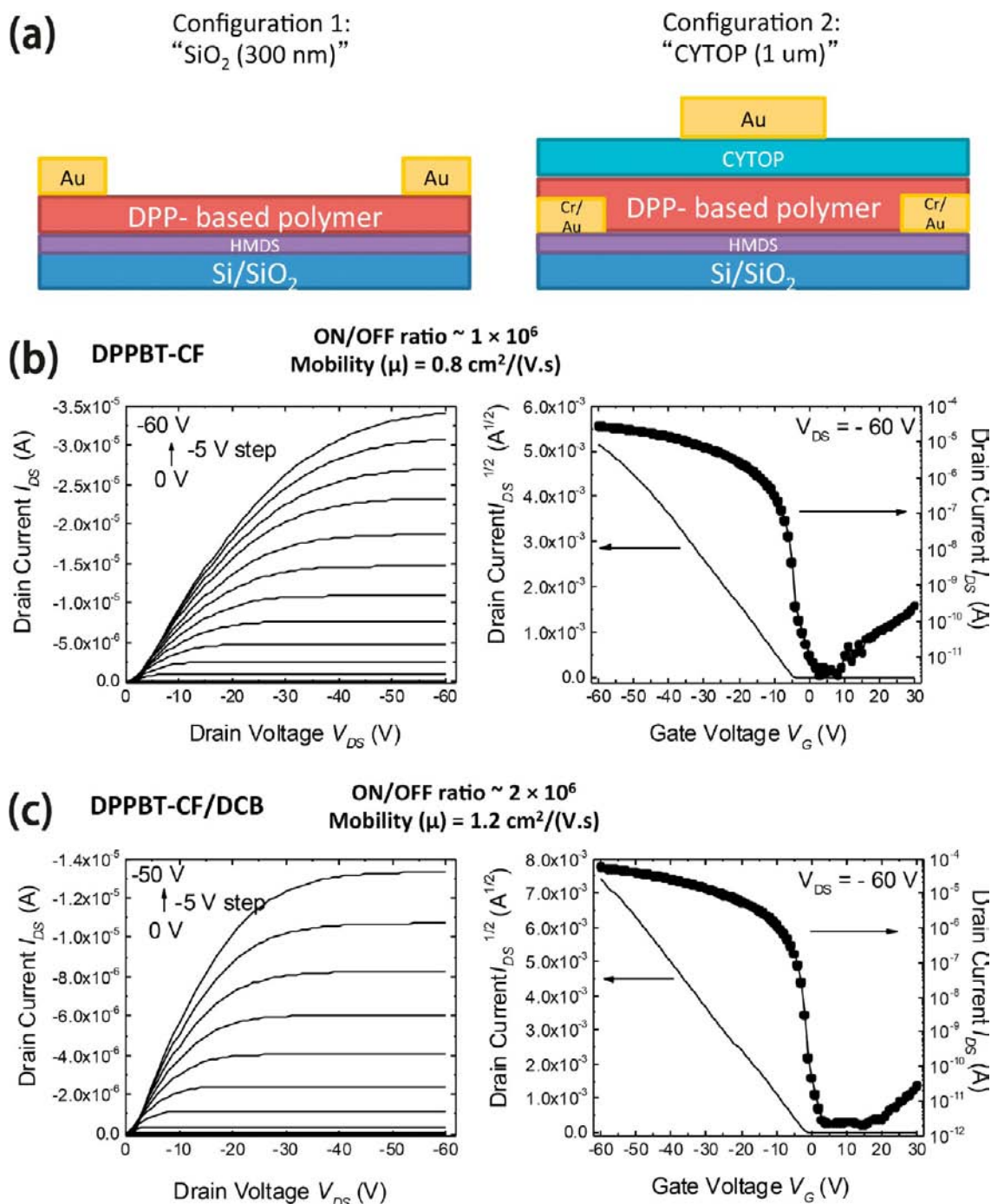
Figure 2. (a) Two OFET device structure; (b) output and transfer curve of DPPBT OFETs device processed from chloroform; (c) output and transfer curve of DPPBT OFETs device processed from chloroform−dichlorobenzene.

Table 1. Summary of Device Performance

| devices	SiO$_2$ (300 nm)		CYTOP (1 um)	
	ON/OFF	mobility (cm^2 V^{-1} s^{-1})	ON/OFF	mobility (cm^2 V^{-1} s^{-1})
DPPF−CB	$(2.3 \pm 0.4) \times 10^3$	0.008 ± 0.001	$(1.1 \pm 0.4) \times 10^3$	0.02 ± 0.005
DPPF−CB/DIO	$(1.2 \pm 0.3) \times 10^5$	0.01 ± 0.008	$(1.3 \pm 0.2) \times 10^4$	0.15 ± 0.022
DPPT−CB	$(1.2 \pm 0.2) \times 10^6$	0.02 ± 0.006	$(1.2 \pm 0.4) \times 10^5$	0.05 ± 0.008
DPPT−CB/DIO	$(3.0 \pm 0.6) \times 10^6$	0.06 ± 0.009	$(1.6 \pm 0.4) \times 10^5$	0.42 ± 0.022
DPPBT−CF	$(1.2 \pm 0.3) \times 10^6$	0.12 ± 0.017	$(1.8 \pm 0.3) \times 10^6$	0.82 ± 0.034
DPPBT−CF/DCB	$(1.1 \pm 0.3) \times 10^7$	0.42 ± 0.024	$(2.4 \pm 0.6) \times 10^6$	1.18 ± 0.096
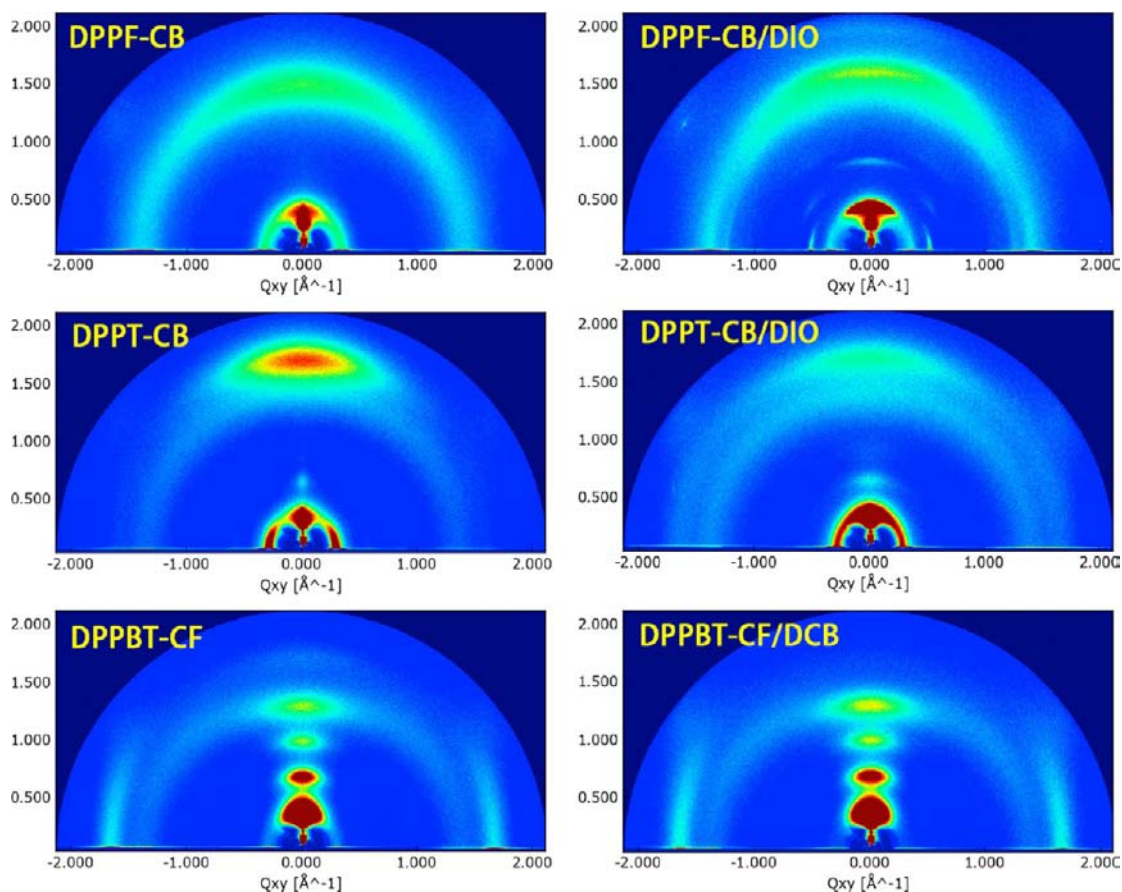
Figure 3. GIXD of DPP polymers on silicon wafer. Polymer thin films were casted from a single solvent and solvent mixtures.

reason for the 6-fold mobility enhancement in the CYTOP devices. For DPPT processed from a single solvent, a face-on orientation was preferred, as evidenced by the strong (010) peak in the out-of-plane direction. A 0.37 nm $\pi-\pi$ stacking distance was observed, which was the shortest in this family. The (100) spacing was ~2.4 nm. The face-on crystal orientation is not in the right direction for charge transport, thus a small mobility (0.05 cm^2 V^{-1} s^{1-}) was obtained. When CB/DIO was used as the processing solvent, the face-on orientation was largely reduced, as seen from the distribution of the (100) peak. When CB was used to spin cast a thin film, the solvent evaporated quickly, and the polymer chains started to order and deposit in the end of solvent evaporation under supersaturation condition. The preferential interaction between the conjugation plane and the substrate gave rise to the preference of a face-on orientation of the polymer crystallites. When processing from CB/DIO mixture, CB evaporates first, resulting in an increased concentration of DIO, a nonsolvent for the polymer. With continued solvent evaporation, the quality of the mixed solvent for the polymer decreases, causing the polymers to aggregate and order, forming a fibrillar type of morphology that assumes an edge-on orientation with respect to the substrate. The aggregation and ordering of the DPP in solution led to a marked enhancement of the ordering in the film and to a 0.42 cm^2 V^{-1} s^{-1} mobility, over an 8-fold increase compared to CB processed thin film. DPPBT showed the highest crystallinity with a strong edge-on crystal orientation. Four orders of diffraction along the (100) direction were evident. The $\pi-\pi$ stacking distance in the in-plane scattering was 0.38 nm. Both crystallinity and crystal orientation

accounted for higher carrier mobilities in this series. The mixed-solvent (CF/DCB) processing slightly increased the edge-on orientation of the crystals, as seen from the azimuthal broadening of the (100) and (010) reflections. This led to mobilities of 1.2 cm^2 V^{-1} s^{-1}. Single-solvent (CF) processed films having a poor orientation had mobilities of 0.8 cm^2 V^{-1} s^{-1}.

Photovoltaic Properties. Solar cells using DPP polymers were fabricated by using polymer:PC$_{71}$BM blends at 1:1 weight ratio. ITO/PEDOT:PSS was used as the anode and LiF/Al was used as the cathode. For low band gap polymers, solvent mixture processing was commonly used to optimize the morphology of the active layer.[25,38] The same mixed-solvent processing protocol as that in OFETs device fabrication was employed in OPV device fabrication (single-solvent processed thin film blends are noted as M1; mixed-solvent processed thin film blends are noted as M2. For DPPF and DPPT blends, chlorobenzne is used as the major solvent, and DIO is used as the additive; for DPPBT blends, chloroform is used as the major solvent, DCB is used as the additive.). As shown in Figure 4 and Table 2, all DPP polymers show a low device performance when processed from a single solvent, due to the smaller short circuit current (J_{sc}). When a mixed-solvent mixture was used, a 5-fold increase in J_{sc} was observed for DPPT and DPPBT blends. The power conversion efficiency (PCE) reached 3.8% for DPPT blends and 5.6% for DPPBT blends. For the DPPBT case, using a solvent mixture to process the blends drastically elevated the incident photon to charge carrier efficiency (IPCE, Figure S2), which is consistent with the observation of the photon current enhancement. For
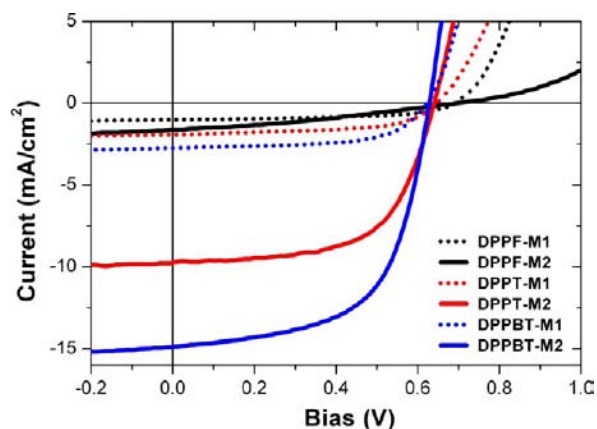
Figure 4. BHJ solar cell devices using DPP polymer:PC$_{71}$BM (1:1 wt) blends as the active layer. For DPPF and DPPT blends, M1:CB; M2:CB/DIO. For DPPBT blends: M1:CF; M2:CF/DCB.

**Table 2. Device Performance of DPP Polymer:PCBM Blends**

devices	Voc (V)	J$_{sc}$ (mA/cm^2)	FF (%)	PCE (%)
DPPF−M1	0.69	1.02	55.5	0.39 (0.56)[a]
DPPF−M2	0.70	1.63	31.5	0.36 (0.45)
DPPT−M1	0.65	1.91	58.2	0.72 (0.90)
DPPT−M2	0.64	9.74	61.2	3.82 (3.85)
DPPBT−M1	0.62	2.75	61.39	1.05 (1.19)
DPPBT−M2	0.63	14.84	60.27	5.62 (5.72)

[a]Maximum performance for the devices.

DPPF, although a slight increase in J_{sc} was observed, the fill factor decreased. Consequently, the PCE remained similar for both processing conditions. These performance differences were highly affected by the thin film morphology.

Structure Order of Blended Thin Film. GIXD was used to assess the ordering in thin films cast from a single solvent, from mixed solvents, and with the use of additives (the same conditions as that in OPV device fabrication). The detailed results are summarized in Figure 5 and Table 3. For the DPPF and DPPBT blends, the crystals assumed an edge-on orientation with the (100) reflection evident in the out-of-plane direction and the (010) peak located in-plane. For the DPPT blends, the opposite held, and the crystals assumed a face-on orientation. For DPPT and DPPBT, the use of an additive led to a narrowing of the (010) reflection (i.e., the persistence of the registration in the (010) direction increased), while the width of the (100) peak increased slightly, indicating a slight reduction in the crystal size along the (100). These changes would be consistent with the formation of a fibrillar type texture, where the (010) is oriented along the fibril axis.

BHJ Thin Film Morphology. In BHJ solar cells, the morphological features are directly correlated to device function. TEM images (Figure 6) show that single-solvent processed thin films exhibit large-scale phase-separated structures (see large TEM images in Figure S3). For DPPF blends, large PCBM-rich domains (dark regions) are seen, 100−200 nm in size. DPPT and DPPBT blends showed similar features. Due to this large-scale phase-separated morphology, device performance was poor. When thin films were processed from a solvent mixture, the morphology was much finer. DPPF (CB/DIO) showed a large dark and bright areas arising either from thickness or density variations. The polymer formed a
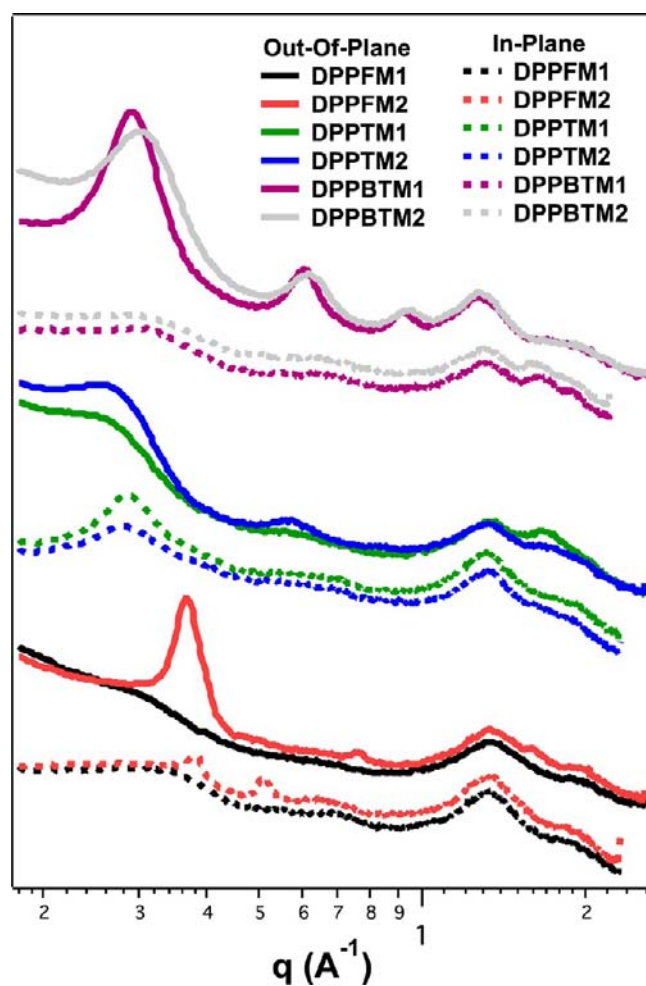
Figure 5. Out-of-plane and in-plane line-cut profiles of polymer:PCBM blends in GIXD. For DPPF and DPPT blends, M1:CB; M2:CB/DIO. For DPPBT blends: M1:CF; M2:CF/DCB.

Table 3. GIXD Results of Polymer−PCBM Blend Thin Films

conditions	(100) (nm)	size (nm)	(010) (nm)	size (nm)
DPPF−M1	1.96	N.A.	N.A.	N.A.
DPPF−M2	1.70	12.8	0.39	4.0
DPPT−M1	2.35	7.6	0.37	1.6
DPPT−M2	2.30	7.2	0.37	2.5
DPPBT−M1	2.24	8.2	0.38	3.0
DPPBT−M2	2.13	6.7	0.39	3.7

mesoporous-like structure, with ∼50 nm spherical aggregates decorating the film. This ill-defined morphology with no well-defined interpenetrating donor−acceptor phases led to poor performance. For the DPPT blends (CB/DIO), a crystalline fibrillar (15−20 nm in diameter) network was observed. The dark area in the interfibrillar regions consists of a PCBM-rich polymer mixture. The size of these PCBM rich areas ranged from tens to hundreds of nanometers. This interpenetrated morphology was favorable for charge transport, especially when the feature size was commensurate with exciton diffusion length, thus maximizing charge carriers and improving device performance. A 5-fold efficiency enhancement was seen for this blend in comparison to the same blend processed from a single-solvent processed film. DPPBT blends processed from a solvent mixture (CF/DCB) show a very small size phase separation.
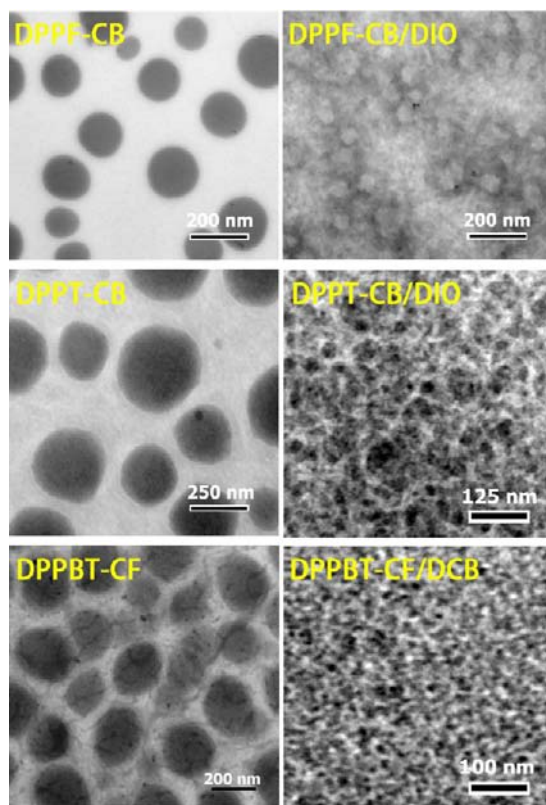
Figure 6. TEM images of polymer:PCBM blends.

Fibrils ~10 nm in diameter were seen with an interfibrillar distance of ~20−50 nm. The interfibrillar regions consisted of a PCBM-rich mixture. In comparison to the DPPT blends, the DPPBT blends showed a smaller size scale of phase separation and fibril width, thus the donor−acceptor interfaces are enlarged, leading to an improved J_{sc} in the devices.

Atomic force microscopy (AFM) was used to study the surface morphology of these thin film samples (Figure 7). Elevations in the topography of a size that corresponded to the dark regions in the TEM micrographs were seen for the single-solvent processed thin films, indicating quite rough surfaces. Consequently, in the TEM images, not only is there contrast from electron density differences but also an apparent contrast from a variation in the film thickness. From the height variations, DPPF blends showed the largest variation (broad humps are observed in the topography) and DPPBT blends showed the least. For thin films processed from a solvent mixture, the surfaces of the DPPF blends wrinkled, with pleats ~50 nm. These could arise from the crystallization of the DPPF at the surface, leading to unfavorable device architectures. In the case of DPPT thin film blends. The surface was smooth with an RMS roughness of 1.8 nm. In the case of DPPBT blends, the surface was even smoother with an RMS roughness of 1.1 nm. In all cases, the surface roughness maps directly onto the sizes of the phase separated domains in the films.

Resonant soft X-ray scattering (RSoXS) was used at an X-ray energy of 284.2 eV, at the carbon K-edge, in order to enhance the contrast of the PCBM-rich region (the X-ray absorption fine structure profiles are shown in Figure S4).[26] The scattering profiles of the blends are summarized in Figure 8. For single-solvent processed thin film blends (Figure 8a), scattering peaks in the very low q region were seen, with corresponding center-to-center distances of domains that correlated well with the domain structure observed by TEM and AFM. Solvent mixture processed thin films had much smaller domains (Figure 8b). For DPPF blends (CB/DIO), a strong peak at 0.0021 A^{-1} was observed (~300 nm), arising from the average center-to-center distance between PCBM-rich domains. From the corresponding TEM images, a general dark−white area separation with similar size scale was seen, supporting the RSoXS results. A shoulder at 0.0071 A^{-1} was observed in the scattering profile, giving a spacing of 88 nm, that most probably comes from the

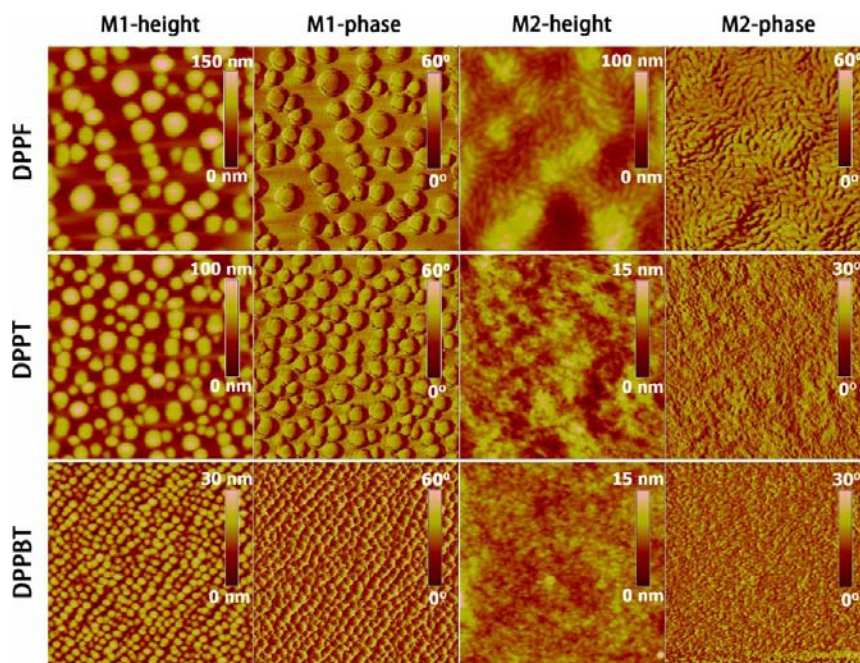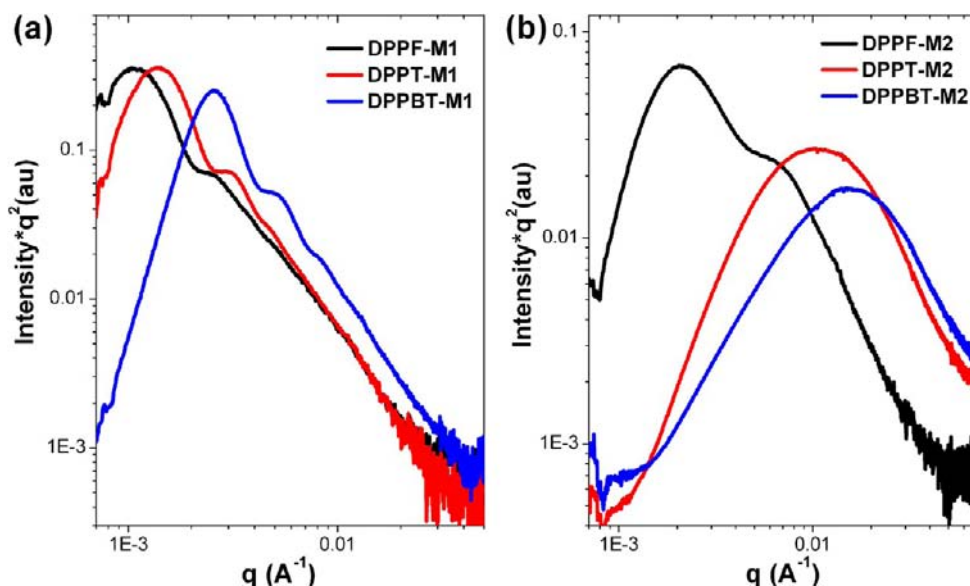**Figure 7.** AFM height and phase images. Single-solvent processed film: 5 μm × 5 μm; solvent mixture processed film: 2 μm × 2 μm. For DPPF and DPPT blends, M1:CB; M2:CB/DIO. For DPPBT blends: M1:CF; M2:CF/DCB.

Figure 8. RSoXS profiles of polymer:PCBM blends casted from (a) single solvent, (b) solvent mixture. For DPPF and DPPT blends, M1:CB; M2:CB/DIO. For DPPBT blends: M1:CF; M2:CF/DCB.

aggregates described previously (see TEM images). When DPPT blends were processed from a solvent mixture (CB/DIO), a broad peak at 0.01 A^{-1} was seen (~63 nm), which can be ascribed to the average fibril−fibril separation distance.[39] For DPPBT blends (CF/DCB), the scattering profile showed a broad peak ~0.016 A^{-1}, corresponding to a distance of 39 nm. With fibrils ~10−20 nm in diameter, this distance correspond to the average fibril−fibril separation distance in these mixtures. Relative to device performance, the scattering and microscopy data indicate that the smaller the size scale of the morphological features, the larger will be the interfacial area, the higher will be J_{sc}, and the better will be the performance. The mixed region between the fibrils could have efficient exciton generation; strong recombination might be a key factor that limits its function. It was pointed out by Janssen and co-workers, for a similar structure to DPPT (also showing a similar morphological picture), that recombination limits the J_{sc} in devices.[23]

The correlation function analysis is applied to analysis the scattering data to providing real space correlations. The correlation function, $\gamma(r)$, is given by

$$\gamma(r) = \frac{\int_0^\infty I(q)q^2\cos(qr)dq}{\int_0^\infty I(q)q^2dq}$$

where $I(q)$ is the scattered intensity at a scattering vector q.

It should be noted that the integrals extend to infinity; consequently, the scattering data were extrapolated to infinity using a damped Porod function.[40] Correlation functions are shown in Figure 9. For DPPF blends, the average hard block thickness (Lc), which is the crystalline part of the conjugated polymer, was estimated by extrapolating the linear region of $\gamma(r)$ to the level of the nadir (as show in Figure 9a, red extrapolating lines), and was ~34.2 nm. The long period (Lp), which corresponds to the average domain spacing of phase separated structure was ~300 nm. For the DPPT blends (CB/DIO), Lc and Lp were 10.4 and 85 nm, respectively; and for the DPPBT blends (CF/DCB), Lc and Lp are 8.2 and 50 nm (Figure 9b). The Lc is smaller than that estimated from the TEM results, which is not surprising because the X-ray data
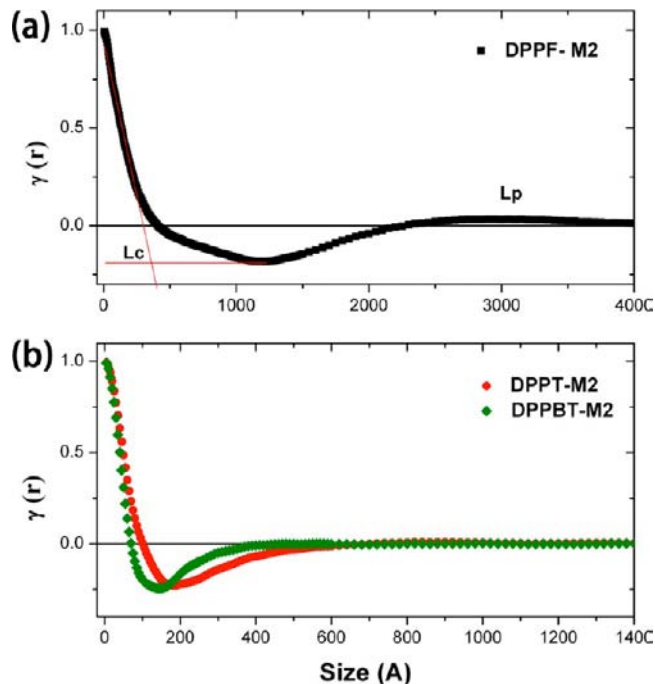
**Figure 9.** Correlation function analysis of RSoXS profiles of polymer:PCBM blends casted from solvent mixture: (a) DPPF−M2; (b) DPPT−M2; and DPPBT−M2. For DPPF and DPPT blends, M1:CB; M2:CB/DIO. For DPPBT blends: M1:CF; M2:CF/DCB.

reflect a volume average over a large area, where the sampling size for TEM is quite small.

Besides the lateral morphology, vertical segregation is also an important factor that influences the device efficiency. In our previous work, we have shown that blends processed from a solvent mixture form a homogeneous film with slight polymer enrichment at the surfaces.[31] Single-solvent processed thin film exhibits a coarse phase separation and, therefore, cannot be homogeneous either in lateral and vertical morphology. Cross-sectional scanning electron microscopy (SEM) was used to study the vertical morphology of these single-solvent processed
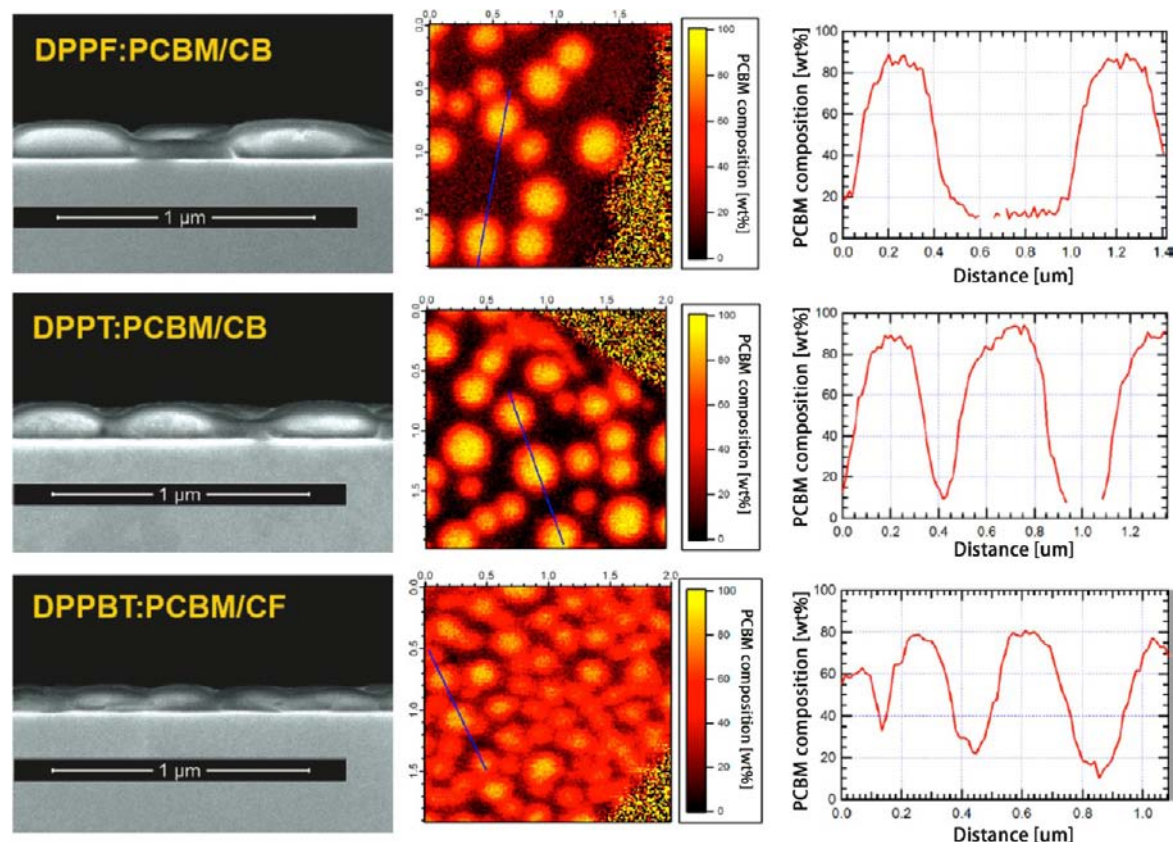
Figure 10. Cross-section SEM image, STXM image, and PCBM compositional analysis of polymer:PCBM blends casted from a single solvent.

films. The results are shown in Figure 10 and Figure S5. For all these three samples, a clear stratified morphology was seen, with bright oval structures buried under a thin gray layer. Those bright ovals are PCBM-rich, while the gray areas are polymer-rich. The scan transition X-ray microscopy (STXM) images are shown beside SEM images, and the color-coding shows the PCBM composition. Similar sizes of PCBM rich domains were observed with STXM. From line-cut profiles of PCBM composition analysis, the bright area in the STXM images contains ~85% PCBM, while the dark regions contains ~12% PCBM. The dark regions between oval structures did not show an obvious PCBM-rich layer; therefore, we can conclude that the PCBM is well-dispersed in the polymer matrix. These values of PCBM in the polymer-rich areas may, in fact, define the limit of miscibility of PCBM in the polymer. In the DPPT blends, the concentration of PCBM in the PCBM-rich domain was ~90%, and in polymer matrix,<10% PCBM. DPPBT blends had higher PCBM region population, as the STXM bright domain contained ~80% of PCBM and dark region contains ~18% of PCBM. From the TEM and SEM images of the films cast from a single solvent, it is evident that the large domains are nearly pure PCBM, indicating that a saturation limit of PCBM in the polymer matrix, forcing the segregation of the PCBM. However, films cast from a solvent mixture showed the formation of a fibrillar network that established a framework in which the remaining materials deposit, leading to a uniform distribution of PCBM in the film.

Commonalities in the Additive Approach. In the previous discussion, we analyzed the effect of additive on the morphology of a series of DPP-based BHJ solar cells. Although a plausible structure−property relationship is established, the use of different solvents makes it difficult to compare the

additive-induced morphology changes directly. Based on this study and previous research,[38,39] the effect of additive should be universal in regulating the morphology of BHJ thin films. Consequently, additional solvents and additives were used to demonstrate the generality of the additive-assisted morphology formation.

Shown in Figure 11 are results for more devices fabricated using DPPT:PCBM blends and DPPBT:PCBM blends. For the DPPT blends, chloroform was used as the solvent, and DIO (3 v%) was used as the additive. For DPPBT blends, chloroform
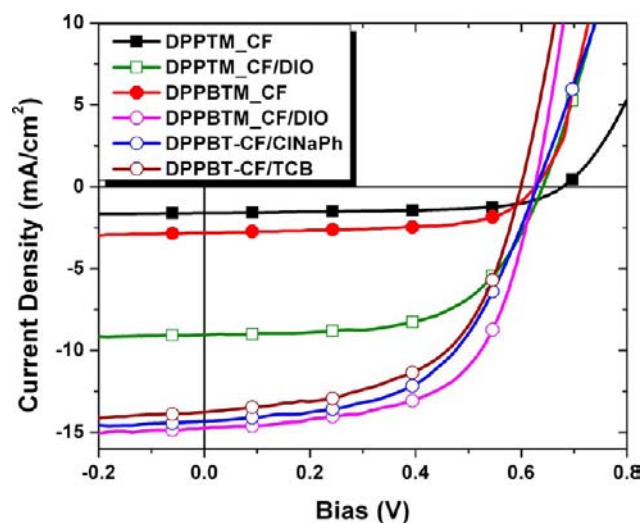
Figure 11. BHJ OPV devices using DPPT blends and DPPBT blends and more solvent-additive processing conditions.

was used as the solvent, DIO (3 v%), and 1-chloronaphthalene (ClNaPh, 5 v%) and 1,2,4-trichlorobenzne (TCB, 5 V%) were used as additives. Detailed results are summarized in Table 4.

Table 4. OPV Device Performance Using Additional Conditions

devices	Voc (V)	J_{sc} (mA/cm^2)	FF (%)	PCE (%)
DPPTM−CF	0.67	1.56	61.4	0.6
DPPTM−CF/DIO	0.64	9.2	59.4	3.4
DPPBTM−CF	0.63	2.62	62.4	1.0
DPPBTM−CF/DIO	0.62	14.33	60.1	5.2
DPPBTM−CF/ClNaPh	0.62	14.31	55.8	4.9
DPPBTM−CF/TCB	0.59	14.1	56.7	4.7

DPPT blends processed from chloroform showed a low current and PCE, which is due to large size scale of the phase-separated morphology, as indicated by the interference maximum seen in the low q region from the RSoXS data (Figure 12). Adding
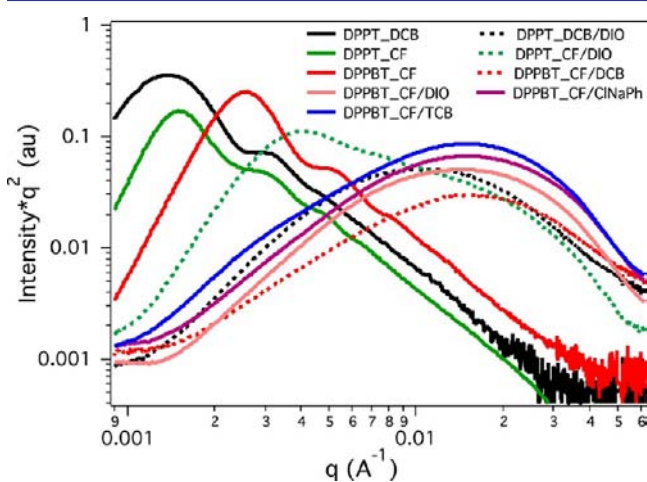

Figure 12. RSoXS profiles of DPPT blends and DPPBT blends using additional solvent-additive processing conditions.

small amounts of DIO in the solution drastically reduced the size scale of the morphology and increased the current to 9.2 mA/cm^2. A broad interference is seen in the scattering data characteristic of a size scale that is similar to that seen for CB/DIO solvent/additive case. An additional interference at ~0.0035 A^{-1} is seen, corresponding to a distance of 180 nm due, more than likely to residual PCBM aggregates that reduced device performance. The DPPBT blends using various additives all showed much-improved J_{sc} in the devices, with differences arising from detailed structural differences. The RSoXS data (Figure 12) showed interferences in a similar scattering vector range, indicating a size scale of the phase-separated morphology that is similar to that seen under CF/DCB processing conditions. When TCB was used as the additive, a weak interference at ~0.003 A^{-1} was seen, corresponding to a distance of 209 nm, arising from PCBM aggregation, which resulted in a slightly reduced device performance. The structural order of these new blends was also studied by GIXD (2D diffraction images and out-of-plane profiles shown in Figures S6 and S7). For DPPT blends, using only chloroform resulted in a face-on orientation that decreased with the addition of DIO. For DPPBT blends, the use of different additives resulted in a reduction in the crystal size

along the (100) direction, which is similar to that seen when CF/DCB was used. The combination of these results clearly demonstrates the commonalities in the use of additives for the preparation of DPP-based BHJ blends, that is, adding additive reduces the size of phase separation as well as modulating the size and orientation of crystallites.

Polarized Scattering and Interfacial Orientation. The lateral morphology of BHJ blends can be probed by various methods. However, the donor−acceptor network interface remains a challenge to characterize. Finding the right probe to capture the localized morphology would be another advancement in understanding the charge segregation, transport, and recombination. When a polarized soft X-ray beam is used, the polarized electrical field plus the component sensitivity enabled new possibilities in exploring interface details.[41−43] Polarized resonant X-ray scattering (PSoXS) experiments, making use of the polarized nature of the synchrotron beam, were performed to elucidate the relative orientation of the components in the active layers. (We primarily focus on a horizontal polarized X-ray beam to perform the experiment. When the X-ray beam was tuned to vertical polarization, complementary scattering image can be obtained.) By tuning the scattering photon energy, localized molecular orientation could be deduced. In this experiment, we took a snapshot of a few typical energies obtained from the near edge X-ray absorption fine structure (NEXAFS) (Figure S4) with the results shown in Figure 13. Here, 284.4 eV is sensitive to PCBM 1s-$\pi^*_{c=c}$ bond transition; 285.4 eV is sensitive to polymer 1s-$\pi^*_{c=c}$ bond transition; 287.4 eV resonance is a combination of carbon−hydrogen, carbon−sulfur, and the Rydberg excitation; and, 291 eV is sensitive to 1s-σ^*_{c-c} bond transition.[28] The scattering intensities at 90° and 180° in the scattering ring were used to assess the strength of anisotropy, by using an anisotropic factor $\sigma = (I_{90} - I_{180})/(I_{90} + I_{180})$. The scattering anisotropy at the different photon energies are shown in Figure 14a.

When DPPT blends were processed from a single solvent (CB), the scattering ring was nearly isotropic at the different photon energies. A slight anisotropy was seen at 285.4 and 287.4 eV. DPPT in blends assume a face-on orientation in the single-solvent processed films. In that orientation, the large π face of the polymer back-bond is perpendicular to the incident X-ray, and the polarized electrical field cannot excite the bond. Consequently, the bond sensitivity was obscured. (A schematic model for this case is shown in Figure S8.) For the mixed-solvent (CB/DIO) processed DPPT blend thin films, the scattering image showed a slight anisotropy at 284.4 eV. When the photon energy was tuned to the polymer 1s-$\pi^*_{c=c}$ bond transition, a clear anisotropy was seen ($\sigma = 0.16$), indicating that the polymer π electron surface could be excited by the polarized electrical field. This was due to the edge-on orientation of the crystallites. When a 287.4 eV photon energy was used, the scattering image became less anisotropic, due to the complicated nature of this absorption band. The scattering at 291 eV was very weak, and no useful information could be obtained. In the DPPBT blends processed from a single solvent (CF), a weak anisotropy was observed at 284.4 eV. This anisotropy was greatly enhanced at 285.4 eV ($\sigma = 0.52$). This was due to the strong edge-on orientation of the polymer crystallites. At 287.4 eV, the strong anisotropy persisted. Yet, at 291 eV, the polarization direction changed ($\sigma = -0.12$). The 291 eV absorption is due to the 1s-σ^*_{c-c} transition, which is geometrically perpendicular to the planes of the π electron cloud, thus it is oriented 90° from the 1s-$\pi^*_{c=c}$ bond transition
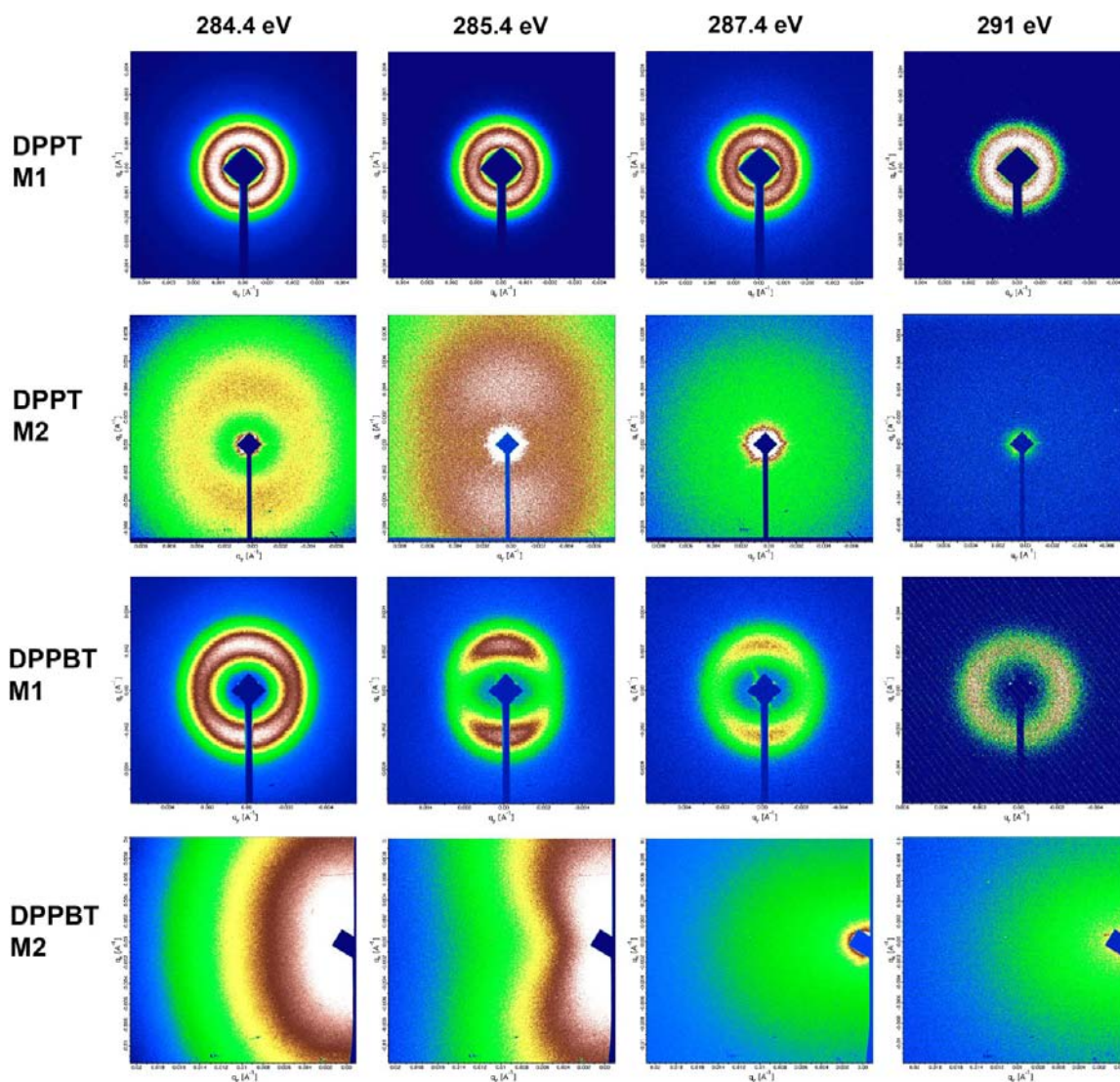
Figure 13. Polarized RSoXS of DPPT/DPPBT:PCBM blends (processed from a single solvent and a solvent mixture) under different photon energies. For DPPF and DPPT blends, M1:CB; M2:CB/DIO. For DPPBT blends: M1:CF, M2:CF/DCB.

polarization. When a solvent mixture (CF/DCB) was used to process the DPPBT blends, the anisotropy persisted. At 285.4 eV, $\sigma = 0.41$ was observed, which was slightly lower than the singl-solvent processed blends. DPPBT−M2 (CF/DCB) thin films were highly edge-on, with a slightly reduced (100) crystal size and orientation in comparison to the DPPBT−M1 (CF) thin film. At 287.4 eV, the polarization changed its direction ($\sigma = -0.10$), which was quite different from DPPBT−M1 sample (CF). The detailed reason for this change was not clear, due to the complexity of the 287.4 eV absorption band. The 1s-$\sigma *_{c—c}$ absorption polarization was also perpendicular to 285.4 eV, the same as in the previous case.

A scheme of morphology is shown in Figure 14b. The chain packing within polymer fibrils is key in dictating the anisotropy in the scattering profiles. The $\pi-\pi$ stacking that is parallel to the electrical field (the $\pi-\pi$ stacking direction is the same with electrical field direction) is excited, leading to a scattering intensity change. (A schematic illustration is shown in Figure 14c.) Fully understanding the scattering polarization and chain packing behavior will require complicated optical models, which is beyond the scope of this discussion. With the current data set, the correlation of TEM image and related PSoXS was

to analyze the scattering anisotropy and interfacial chain orientation relationship. We saw fiber network structures in the BHJ blends, and the fiber-to-fiber distance dictates the scattering profiles. As seen from the scattering anisotropy at the polymer resonance band, if the polymer chain is oriented parallel to the fibril axis, the type 1 chain packing, the polarized nature of the incident X-ray beam would lead to a reduced intensity in the electrical field direction, giving rise to the 285.4 eV scattering image (the intensity enhanced in vertical direction, the electrical field is in horizontal direction). If the polymer chain is oriented orthogonal to the fibril axis, the type 2 chain packing, which is commonly seen in P3HT nanofibrils, the polarized electrical field would lead to an intensity enhancement perpendicular to electrical field direction. Consequently, the orientation of the chain axis can be determined from the azimuthal dependence of the PSoXS profile. It was, however, difficult to correlate that orientation with the device performance.

■ CONCLUSION

We have investigated the relationship of DPP-based low band gap polymers and processing conditions to morphology and
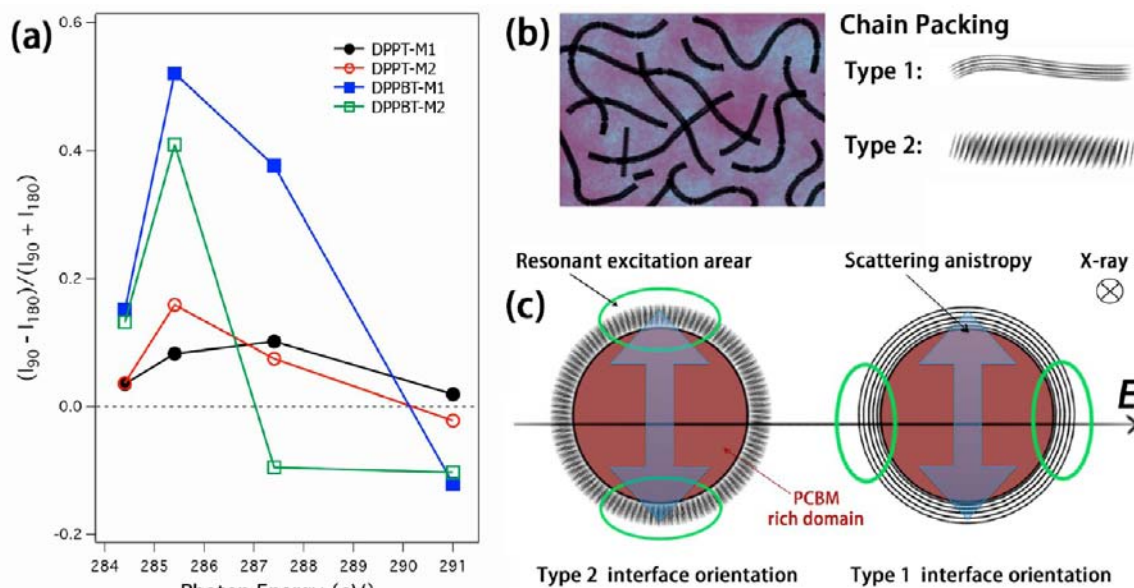
Figure 14. (a) Anisotropy of DPPT/DPPBT:PCBM blends; (b) scheme of typical fibril mesh BHJ morphology and two possible chain alignment in fibrils; (c) schematic illustration of the scattering anisotropy.

performance in OFETs and OPVs. Various techniques have been used to probe the morphological details of the pure films and BHJ blends. These morphological features have been correlated with the device performance and chemical structure of the DPP polymers. By slightly changing the chemical structure (e.g., from a DPP−thiophene copolymer to a DPP−bithiophene copolymer), the crystal orientation, crystal size, and domain size change markedly, indicating that full optimization of OFET and OPV performance must include both device engineering and material optimization. We have shown that the crystal orientation strongly influences the transport properties in OFETs. In OPVs, crystalline fibrils are an important factor for high efficiency devices. These crystalline structures are sensitive to processing conditions. Processing conditions also influence the morphology of polymer:PCBM blends. Thin film blends cast from a single solvent show a large-scale phase separation and a stratified morphology normal to the film surface. Fairly pure PCBM aggregates that were surrounded by the polymer matrix were observed. The use of additives in the casting solvents fundamentally changed the thin film morphology. With the presence of a selective solvent additive, the crystallization of conjugated polymers is altered, as can be seen from the difference in crystal size and orientation. At the same time, the solvent additive changed the film-drying process, enabling PCBM to be uniformly distributed within the film. The combination of these two effects leads to a smooth thin film, with crystalline polymer fibrils forming a network, with a mixture of PCBM and the polymer being deposited inside the mesh of the network. Tuning the size of this network structure by using additives is one route to further enhance device performance. The network structure and nature of the PCBM -rich regions are affected by the detailed chemical structure of the polymer, as seen in the results of DPPT and DPPBT. Therefore, it is essential to quantify the morphological details and the function of each phase. By gaining a fundamental knowledge of the chemical physics of the polymer−particle mixture, higher efficiency devices can be realized.

■ ASSOCIATED CONTENT

ⓢ Supporting Information
Experimental details and additional figures. This material is available free of charge via the Internet at http://pubs.acs.org.

■ AUTHOR INFORMATION

Corresponding Authors
*E-mail: abriseno@mail.pse.umass.edu (A.L.B.).
*E-mail: tom.p.russell@gmail.com (T.P.R.).
Notes
The authors declare no competing financial interest.

■ ACKNOWLEDGMENTS

■ REFERENCES

(1) He, Z.; Zhong, C.; Su, S.; Xu, M.; Wu, H.; Cao, Y. *Nat. Photon.* **2012**, *6*, 593−597.
(2) Li, J.; Zhao, Y.; Tan, H. S.; Guo, Y.; Di, C.-A.; Yu, G.; Liu, Y.; Lin, M.; Lim, S. H.; Zhou, Y.; Su, H.; Ong, B. S. *Sci. Rep.* **2012**, *2*, 754.
(3) Bian, L.; Zhu, E.; Tang, J.; Tang, W.; Zhang, F. *Prog. Polym. Sci.* **2012**, *37*, 1292−1331.
(4) Dennler, G.; Scharber, M. C.; Ameri, T.; Denk, P.; Forberich, K.; Waldauf, C.; Brabec, C. J. *Adv. Mater.* **2008**, *20*, 579−583.
(5) Zhou, H.; Yang, L.; You, W. *Macromolecules* **2012**, *45*, 607−632.
(6) Huo, L.; Hou, J. *Polym. Chem.* **2011**, *2*, 2453−2461.
(7) Liu, F.; Gu, Y.; Jung, J. W.; Jo, W. H.; Russell, T. P. *J. Polym. Sci., Part B: Polym. Phys.* **2012**, *50*, 1018−1044.

19258

dx.doi.org/10.1021/ja408923y | *J. Am. Chem. Soc.* 2013, 135, 19248−19259

(8) Rivnay, J.; Toney, M. F.; Zheng, Y.; Kauvar, I. V.; Chen, Z.; Wagner, V.; Facchetti, A.; Salleo, A. *Adv. Mater.* **2010**, *22*, 4359−4363.

(9) Tsao, H. N.; Cho, D.; Andreasen, J. W.; Rouhanipour, A.; Breiby, D. W.; Pisula, W.; Müllen, K. *Adv. Mater.* **2009**, *21*, 209−212.

(10) Ong, B. S.; Wu, Y.; Liu, P.; Gardner, S. *Adv. Mater.* **2005**, *17*, 1141−1144.

(11) Kim, D. H.; Lee, B.-L.; Moon, H.; Kang, H. M.; Jeong, E. J.; Park, J.-I.; Han, K.-M.; Lee, S.; Yoo, B. W.; Koo, B. W.; Kim, J. Y.; Lee, W. H.; Cho, K.; Becerril, H. A.; Bao, Z. *J. Am. Chem. Soc.* **2009**, *131*, 6124−6132.

(12) Joseph Kline, R.; McGehee, M. D.; Toney, M. F. *Nat. Mater.* **2006**, *5*, 222−228.

(13) Sirringhaus, H.; Brown, P. J.; Friend, R. H.; Nielsen, M. M.; Bechgaard, K.; Langeveld-Voss, B.; Spiering, A.; Janssen, R. A. J.; Meijer, E. W.; Herwig, P. *Nature* **1999**, *401*, 685−688.

(14) Shtein, M.; Mapel, J.; Benziger, J. B.; Forrest, S. R. *Appl. Phys. Lett.* **2002**, *81*, 268−270.

(15) Salleo, A.; Chabinyc, M. L.; Yang, M. S.; Street, R. A. *Appl. Phys. Lett.* **2002**, *81*, 4383−4385.

(16) Veres, J.; Ogier, S.; Lloyd, G. *Chem. Mater.* **2004**, *16*, 4543−4555.

(17) Yoon, M.-H.; Kim, C.; Facchetti, A.; Marks, T. J. *J. Am. Chem. Soc.* **2006**, *128*, 12851−12869.

(18) Thompson, B. C.; Fréchet, J. M. J. *Angew. Chem., Int. Ed.* **2008**, *47*, 58−77.

(19) Brabec, C. J.; Gowrisanker, S.; Halls, J. J. M.; Laird, D.; Jia, S.; Williams, S. P. *Adv. Mater.* **2010**, *22*, 3839−3856.

(20) Bijleveld, J. C.; Zoombelt, A. P.; Mathijssen, S. G. J.; Wienk, M. M.; Turbiez, M.; de Leeuw, D. M.; Janssen, R. A. J. *J. Am. Chem. Soc.* **2009**, *131*, 16616−16617.

(21) Bronstein, H.; Chen, Z.; Ashraf, R. S.; Zhang, W.; Du, J.; Durrant, J. R.; Shakya Tuladhar, P.; Song, K.; Watkins, S. E.; Geerts, Y.; Wienk, M. M.; Janssen, R. A. J.; Anthopoulos, T.; Sirringhaus, H.; Heeney, M.; McCulloch, I. *J. Am. Chem. Soc.* **2011**, *133*, 3272−3275.

(22) Hou, J.; Chen, H.-Y.; Zhang, S.; Li, G.; Yang, Y. *J. Am. Chem. Soc.* **2008**, *130*, 16144−16145.

(23) Li, W.; Roelofs, W. S. C.; Wienk, M. M.; Janssen, R. A. J. *J. Am. Chem. Soc.* **2012**, *134*, 13787−13795.

(24) Bijleveld, J. C.; Gevaerts, V. S.; Di Nuzzo, D.; Turbiez, M.; Mathijssen, S. G. J.; de Leeuw, D. M.; Wienk, M. M.; Janssen, R. A. J. *Adv. Mater.* **2010**, *22*, E242−E246.

(25) Wienk, M. M.; Turbiez, M.; Gilot, J.; Janssen, R. A. J. *Adv. Mater.* **2008**, *20*, 2556−2560.

(26) Ye, L.; Zhang, S.; Ma, W.; Fan, B.; Guo, X.; Huang, Y.; Ade, H.; Hou, J. *Adv. Mater.* **2012**, *24*, 6335−6341.

(27) Li, Y.; Sonar, P.; Singh, S. P.; Soh, M. S.; van Meurs, M.; Tan, J. *J. Am. Chem. Soc.* **2011**, *133*, 2198−2204.

(28) Zhang, X.; Richter, L. J.; DeLongchamp, D. M.; Kline, R. J.; Hammond, M. R.; McCulloch, I.; Heeney, M.; Ashraf, R. S.; Smith, J. N.; Anthopoulos, T. D.; Schroeder, B.; Geerts, Y. H.; Fischer, D. A.; Toney, M. F. *J. Am. Chem. Soc.* **2011**, *133*, 15073−15084.

(29) Li, Y.; Singh, S. P.; Sonar, P. *Adv. Mater.* **2010**, *22*, 4862−4866.

(30) Dou, L.; You, J.; Yang, J.; Chen, C.-C.; He, Y.; Murase, S.; Moriarty, T.; Emery, K.; Li, G.; Yang, Y. *Nat. Photon.* **2012**, *6*, 180−185.

(31) Liu, F.; Gu, Y.; Wang, C.; Zhao, W.; Chen, D.; Briseno, A. L.; Russell, T. P. *Adv. Mater.* **2012**, *24*, 3947−3951.

(32) Spano, F. C. *Acc. Chem. Res.* **2010**, *43*, 429−439.

(33) Zaumseil, J.; Sirringhaus, H. *Chem. Rev.* **2007**, *107*, 1296−1323.

(34) Wei, Q.; Miyanishi, S.; Tajima, K.; Hashimoto, K. *ACS Appl. Mater. Interfaces* **2009**, *1*, 2660−2666.

(35) Sirringhaus, H. *Adv. Mater.* **2005**, *17*, 2411−2425.

(36) Mannsfeld, S. C. B.; Tang, M. L.; Bao, Z. *Adv. Mater.* **2010**, *23*, 127−131.

(37) Kline, R. J.; DeLongchamp, D. M.; Fischer, D. A.; Lin, E. K.; Richter, L. J.; Chabinyc, M. L.; Toney, M. F.; Heeney, M.; McCulloch, I. *Macromolecules* **2007**, *40*, 7960−7965.

(38) Lee, J. K.; Ma, W. L.; Brabec, C. J.; Yuen, J.; Moon, J. S.; Kim, J. Y.; Lee, K.; Bazan, G. C.; Heeger, A. J. *J. Am. Chem. Soc.* **2008**, *130*, 3619−3623.

(39) Gu, Y.; Wang, C.; Russell, T. P. *Adv. Energy Mater.* **2012**, *2*, 683−690.

(40) Ryan, A. J.; Hamley, I. W.; Bras, W.; Bates, F. S. *Macromolecules* **1995**, *28*, 3860−3868.

(41) Gann, E.; Young, A. T.; Collins, B. A.; Yan, H.; Nasiatka, J.; Padmore, H. A.; Ade, H.; Hexemer, A.; Wang, C. *Rev. Sci. Instrum.* **2012**, *83*, 045110.

(42) Collins, B. A.; Cochran, J. E.; Yan, H.; Gann, E.; Hub, C.; Fink, R.; Wang, C.; Schuettfort, T.; McNeill, C. R.; Chabinyc, M. L.; Ade, H. *Nat. Mater.* **2012**, *11*, 536−543.

(43) Ma, W.; Tumbleston, J. R.; Wang, M.; Gann, E.; Huang, F.; Ade, H. *Adv. Energy Mater.* **2013**, *3*, 864−872.